Towards understanding global variability in ocean carbon-13

Alessandro Tagliabue[1] and Laurent Bopp[1]

Received 18 June 2007; revised 8 November 2007; accepted 27 November 2007; published 8 March 2008.

[1] We include a prognostic parameterization of carbon-13 into a global ocean-biogeochemistry model to investigate the spatiotemporal variability in ocean carbon-13 between 1860 and 2000. Carbon-13 was included in all 10 existing carbon pools, with dynamic fractionations occurring during photosynthesis, gas exchange and carbonate chemistry. We find that ocean distributions of $\delta^{13}C_{DIC}$ at any point in time are controlled by the interplay between biological fractionation, gas exchange, and ocean mixing. In particular, the deep ocean $\delta^{13}C_{DIC}$ is sensitive (by > 0.5‰) to the degree of ocean ventilation. On interannual timescales, although the variability in $\delta^{13}C_{DIC}$ is a first order function of the atmospheric $\delta^{13}CO_2$ and overall carbon flux, the spatial distributions are controlled by the degree to which surface waters are exposed to the atmosphere. The $\delta^{13}C_{POC}$ is highly sensitive to the species of inorganic carbon assimilated during photosynthesis (by 10 to 17‰), as well as the intrinsic growth rate and in situ [CO_2(aq)], suggesting that phytoplankton utilize both HCO_3^- and CO_2(aq). The relationship between $\Delta\delta^{13}C_{DIC}$ and anthropogenic carbon (C_{ant}) varies by ±70% regionally and circulation and biotic effects can influence estimates of C_{ant} that are based on $\Delta\delta^{13}C_{DIC}$.

Citation: Tagliabue, A., and L. Bopp (2008), Towards understanding global variability in ocean carbon-13, *Global Biogeochem. Cycles*, *22*, GB1025, doi:10.1029/2007GB003037.

1. Introduction

[2] The stable isotopes of carbon (^{12}C and ^{13}C) can be used as tracers of carbon cycle processes across multiple timescales. The ^{13}C isotopic composition of ocean dissolved inorganic C (DIC) is evaluated relative to the PDB standard ($\delta^{13}C_{DIC}$) and is typically between 0.5 and 2.5‰ in the modern surface ocean [e.g., *Gruber et al.*, 1999]. Since the industrial revolution, the combustion of isotopically light organic C pools has markedly reduced atmospheric $\delta^{13}CO_2$ and, as a consequence, the mean ocean $\delta^{13}C_{DIC}$, allowing researchers to infer the oceanic uptake of anthropogenic CO_2 to be between 1.9 and 2.1 Pg C a^{-1} between the 1970s and the 1990s [e.g., *Quay et al.*, 1992, 2007; *Tans et al.*, 1993; *Ciais et al.*, 1995; *Heimann and Maier-Reimer*, 1996; *Gruber et al.*, 1999; *Sonnerup et al.*, 1999; *Gruber and Keeling*, 2001]. As the $\delta^{13}C_{DIC}$ signal is retained during the precipitation of calcite and aragonite by calcareous plankton and corals it can also provide information on carbon cycling and ocean circulation across paleo timescales [e.g., *Lynch-Stieglitz et al.*, 2007]. Additionally, the isotopic composition of particulate organic C (POC, $\delta^{13}C_{POC}$) will reflect the conditions under which photosynthetic carbon fixation occurs [*Farquhar et al.*, 1982] and might permit the reconstruction of past ocean CO_2(aq) concentrations [*Popp et al.*, 1997]. The relative contributions of ^{12}C and ^{13}C to a given ocean C pool (DIC or POC) are controlled by the external sources and sinks, as well as chemical and biological fractionation.

[3] A major control on ocean $\delta^{13}C_{DIC}$ and $\delta^{13}C_{POC}$ is the fractionation that occurs when inorganic carbon is assimilated by phytoplankton during photosynthesis (ε_p). In general, ε_p is between 5‰ and 27‰ and depends on the CO_2(aq) concentration, intracellular CO_2, cell wall permeability, as well as the method of C uptake [*Raven and Johnston*, 1991; *Laws et al.*, 1995, 1997; *Rau et al.*, 1996; *Popp et al.*, 1998, 1999; *Cassar et al.*, 2004]. Under laboratory conditions, ε_p is positively and negatively related to the seawater CO_2(aq) concentration and the phytoplankton specific growth rate (μ), respectively, as well as reaching a minimum at high values of μ/CO_2(aq) [*Laws et al.*, 1995, 1997; *Burkhardt et al.*, 1999]. Field and laboratory studies have further shown that ε_p is inversely correlated with the phytoplankton surface area to volume ratio [*Popp et al.*, 1998, 1999; *Burkhardt et al.*, 1999; *Trull and Armand*, 2001]. Last, the means by which phytoplankton transport inorganic C to Rubsico (either diffusion of CO_2(aq) or active uptake/extracellular conversion of HCO_3^-) can cause additional variability in ε_p [*Cassar et al.*, 2004]. Overall, $\delta^{13}C_{POC}$ typically varies between −16 and −36 ‰ [*Goericke and Fry*, 1994].

[4] Despite being quantitatively less important than biological cycling, fractionation during gas exchange and DIC chemistry is also an important control on $\delta^{13}C_{DIC}$. The overall fractionation during gas exchange depends on the fractionation of ^{13}C between the various C species that make up DIC, as well as that due to kinetic gas transfer and dissolution factors [*Zhang et al.*, 1995]. The total fractionation during CO_2 invasion is generally between 2.4 and 3‰

[1]Laboratoire des Sciences du Climat et de l'Environnement, IPSL-CEA-CNRS-UVSQ Orme des Merisiers, Gif sur Yvette, France.

0886-6236/08/2007GB003037

[*Wanninkhof*, 1985; *Zhang et al.*, 1995], while that resulting from DIC chemistry is temperature dependant (increasing $\delta^{13}C_{DIC}$ in cold waters and vice versa) and between 8 and 10.5‰ [*Zhang et al.*, 1995]. The impact of gas exchange on $\delta^{13}C_{DIC}$ depends on the residence time of ocean surface waters. Finally, ocean ^{13}C distributions are also modified by ocean circulation and mixing.

[5] Understanding the factors that contribute to variability in ocean $\delta^{13}C$ is important in evaluating modern spatiotemporal distributions of $\delta^{13}C$, as well as long term geologic records. In this study, we include a prognostic description of the cycle of ^{13}C within the Pelagic Integration Scheme for Carbon and Ecosystem studies (PISCES) global ocean-biogeochemistry model [*Aumont and Bopp*, 2006] and conduct simulations under a constant ocean circulation from 1860 to 2000 that are forced by observed values of atmospheric CO_2 and $\delta^{13}CO_2$. Specifically, we appraise the role of physical and biological factors in controlling the surface and deep distributions of ocean $\delta^{13}C$, as well as the processes governing the temporal changes in ocean ^{13}C pools over century timescales. We draw attention to the importance of deep ventilation near the Antarctic continental shelf in setting the deep ocean $\delta^{13}C_{DIC}$. In addition, the degree of partitioning of ^{13}C between dissolved and particulate pools is found to be dependant on the form of inorganic C used in photosynthesis. We also examine how the relationship between anthropogenic carbon (C_{ant}) and changes in $\delta^{13}C_{DIC}$ compares to those derived from the earlier generation ocean-biogeochemistry model of *Heimann and Maier-Reimer* [1996]. While the overall historical trend in ocean $\delta^{13}C$ is function of the net air-sea CO_2 flux and the atmospheric $\delta^{13}CO_2$, observed changes in $\delta^{13}C_{DIC}$ will reflect contributions from biotic and circulation effects, as well as C_{ant}.

2. Methods

2.1. The PISCES Model

[6] The PISCES ocean-ecosystem model is extensively described by *Aumont and Bopp* [2006]. In brief, PISCES includes two phytoplankton functional groups (nanophytoplankton and diatoms), meso- and micro-zooplankton, 2 detrital size classes, calcium carbonate, DIC, CO_3^{2-}, dissolved organic C, nitrate (NO_3), phosphate (PO_4), Silicic acid ($Si(OH)_4$), and iron (Fe) [*Aumont and Bopp*, 2006]. Fixed 'Redfield' ratios are employed for NO_3 and PO_4, while the ratios of both Si, and Fe, to C vary dynamically as a function of the phytoplankton functional group and environmental variables. Air-sea gas exchange of CO_2(aq) utilizes the quadratic parameterization of the wind speed dependence of the piston velocity [*Wanninkhof*, 1992]. PISCES has already been validated and employed for a wide range of studies [e.g., *Bopp et al.*, 2005; *Aumont and Bopp*, 2006; *Tagliabue et al.*, 2008] and is therefore an ideal platform for investigating the spatial and temporal variability in $\delta^{13}C$ on decadal timescales [e.g., *Rodgers et al.*, 2008].

[7] The physical model coupled to PISCES is based on the ORCA2 global ocean model configuration of OPA version 8.2 [*Madec et al.*, 1998] and also includes a dynamic-thermodynamic sea ice model [*Timmermann et al.*, 2003]. The mean horizontal resolution is approximately 2° by 2° cos latitude and the meridional resolution is enhanced to 0.5° at the equator. The model has 30 vertical levels, with an increment that increases from 10m at the surface to 500 m at depth (12 levels are located in the first 125 m).

[8] Our standard physical model employs climatological atmospheric forcing from various data sets. These include NCEP/NCAR 2m atmospheric temperature (averaged between 1948 and 2003) and relative humidity, ISCCP total cloudiness (averaged between 1983 and 2001), precipitation (averaged between 1979 and 2001), weekly wind stress based on ERS and TAO observations and creates a representation of ocean circulation/mixing that is forced by observational climatologies. Please see *Aumont and Bopp* [2006] for more details and the associated references.

2.2. ^{13}C Parameterization

[9] We explicitly resolve ^{13}C in the existing 3 dissolved and 7 particulate C pools, with fractionation occurring during photosynthesis, precipitation of calcite, gas exchange and carbonate chemistry. We parameterize ε_p (‰), via the empirical relationship of *Laws et al.* [1995], to be a function of the CO_2(aq) concentration (μmol kg^{-1}) and the specific growth rate (μ_i, d^{-1}) of each phytoplankton group *i*.

$$\varepsilon_{pi} = \left(\left({}^{\mu_i}\Big/_{CO_{2(aq)}} \right) - 0.371 \right) \Big/ -0.015 \quad (1)$$

[10] In an attempt to account for the influence of cell size on ε_p [*Popp et al.*, 1998, 1999; *Trull and Armand*, 2001], as well as the observed minimum at high values of μ/CO_2(aq) [*Laws et al.*, 1997], we restrict the variation in ε_p to between 5 and 20, and 10 and 26‰ for diatoms and nanophytoplankton, respectively. Under our standard conditions we assume the rate of change in DIC^{13} into POC^{13} for phytoplankton group i(F_{POC13i}) is a function of net primary production (NPP_i, mol C m^{-3} s^{-1}), ε_{pi}, and the seawater ratio of DIC^{13} to DIC^{12} (R_{DIC}).

$$F_{POC13i} = NPP_i^* \left(1 - \left({}^{\varepsilon_{pi}}\Big/_{1000} \right) \right) * R_{DIC} \quad (2)$$

[11] Calcite formation has a fixed fractionation of 1‰ and is related to R_{DIC}. Fractionation during gas exchange, and the conversion of CO_2(aq) to DIC, are represented using the equations of *Zhang et al.* [1995] and are a function of temperature and the proportion of the DIC present as CO_3^{2-}.

2.3. Model Experiments

[12] The physical circulation and climatological forcings (atmospheric temperature, relative humidity, cloudiness, precipitation, dust and wind stress) are unchanged for the duration of our study. Prior to the experimental runs, PISCES (including the new ^{13}C parameterization) was spun

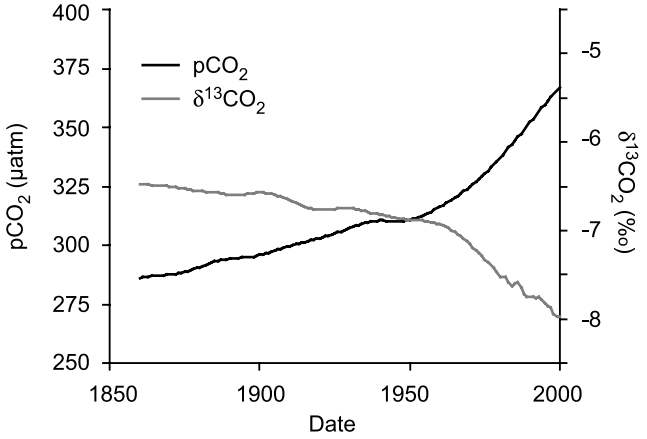

Figure 1. The temporal evolution of the atmospheric pCO_2 (μatm) and $\delta^{13}CO_2$ (‰) from 1860 to 2000 used in this study.

up for 3000 years under preindustrial conditions. By this time, the average drift (i.e., during final 200 years of the model spin up) in the air-sea $^{12}CO_2$ and $^{13}CO_2$ fluxes were 0.07 Pg ^{12}C a^{-1} $century^{-1}$ and 0.09 Gg ^{13}C a^{-1} $century^{-1}$, respectively. Alternatively, the drift in the deep Pacific ocean $\delta^{13}C_{DIC}$ was 0.015 ‰ $century^{-1}$, while in the North Atlantic it was 0.002 ‰ $century^{-1}$. We then forced PISCES with yearly atmospheric pCO_2 (μatm) [*Keeling et al.*, 2001] and $\delta^{13}CO_2$ (‰) data [*Francey et al.*, 1999; *Keeling et al.*, 2001] from 1860 to 2000 (see Figure 1, denoted PISCES-A). To appraise the relative contributions of atmospheric pCO_2 and $\delta^{13}CO_2$ to variability in $\delta^{13}C_{DIC}$ we also performed an experiment where only atmospheric pCO_2 varied ($\delta^{13}CO_2$ was fixed to the 1860 value, denoted PISCES-B). Additionally, a control simulation was conducted over the same time period, with atmospheric pCO_2 and $\delta^{13}CO_2$ fixed at 1860 levels (denoted PISCES-E).

[13] In order to asses the impact of assuming that phytoplankton only transport CO_2(aq), we assumed that the cellular transport of ^{13}DIC (equation (2)) is related to the seawater ratio of $^{13}CO_2$(aq) to $^{12}CO_2$(aq) ($R_{CO2(aq)}$, denoted PISCES-C). This was achieved by calculating $^{13}CO_2$(aq) concentration from temperature and $\delta^{13}C_{DIC}$ following *Rau et al.* [1996] alongside the $^{12}CO_2$(aq) concentration already calculated in PISCES. In all other cases, we assume that phytoplankton transport DIC, which is akin to assuming virtually 100% of uptake from the bicarbonate pool. We also ran simulations that utilized an alternative representation of ocean physics, thereby allowing us to appraise the role of ocean circulation in controlling $\delta^{13}C_{DIC}$ (PISCES-D). In this simulation, the IPSL-CM4 coupled ocean-atmosphere model [*Marti et al.*, 2005] was integrated for 300 years under pre industrial conditions and produced monthly climatologies that were used to drive PISCES offline [*Bopp et al.*, 2005]. Both PISCES-C and PISCES-D were spun up for 3000 years under preindustrial conditions and then integrated from 1860 to 2000 forced by historical atmospheric pCO_2 and $\delta^{13}CO_2$ (Figure 1). For completeness, all model experiments are summarized in Table 1.

3. Results and Discussion

3.1. Surface Water Distributions of $\delta^{13}C_{DIC}$ and $\delta^{13}C_{POC}$

[14] Annually averaged surface water distributions of $\delta^{13}C_{DIC}$ from 1990 (Figure 2a) compare well with the compendium of observations (between 1978 and 1997) reported by *Gruber et al.* [1999]. Although PISCES does a good job of representing the inter-basin trends in $\delta^{13}C_{DIC}$, the absolute values are generally approximately 0.2‰ too low, especially in North Pacific gyre (Figures 3, 4a and 4b and Table 2). At high latitudes, the differences between PISCES and observations is likely due to the seasonality in primary production, which results in $\delta^{13}C_{DIC}$ varying by as much as 0.5 and 1‰ in the Atlantic and Pacific Ocean, respectively (Figures 4a and 4b). The greatest seasonal variability in $\delta^{13}C_{DIC}$ is at Southerly high latitudes (Figures 4a and 4b) and is due to the elevated biological productivity that occurs on the Antarctic continental shelf during the austral spring and summer. The large negative excursion around 0° in Figure 4a is due to the Amazon outflow, which has very low $\delta^{13}C_{DIC}$ values, but only occupies a small geographic area (see Figure 2a), whereas in Figure 4b the low $\delta^{13}C_{DIC}$ values in the east equatorial Pacific are represented by the data (Figures 4b and 2a). At low latitudes, especially in sub tropical gyres, the model underestimates surface $\delta^{13}C_{DIC}$ (Figures 4a and 4b and Table 2), which is most likely a result of observations being collected between 1978 and 1997, a period over which the mean ocean $\delta^{13}C_{DIC}$ has declined by approximately 0.3‰ [*Gruber et al.*, 1999]. In the Indian Ocean basin, PISCES does an excellent job of reproducing $\delta^{13}C_{DIC}$ observations (Figure 2a). Overall, while PISCES-A accounts for around 60% of the observed $\delta^{13}C_{DIC}$ standard deviation (for the year 1990, Figure 3, Table 2), it should be noted that the standard deviation of the data also includes the contribution of interannual variability between 1978 and 1997.

[15] Surface distributions of $\delta^{13}C_{DIC}$ reflect the contributions of biological fractionation, gas exchange and ocean circulation. For example, seasonally high values of $\delta^{13}C_{DIC}$ at the highest latitudes, especially at the Polar Front and near the Antarctic shelf (Figures 4a and 4b) reflect fractionation during primary production. While one would expect upwelling zones to reflect the introduction of "light" DIC (from remineralization of POC^{13}), it is also important

Table 1. A Summary of the Experiments Conducted in This Study

Model Exp.	Change With Time? pCO_2	Change With Time? $\delta^{13}CO_2$	C_{inorg} Uptake	Circulation
PISCES-A	yes	yes	R_{DIC}	standard
PISCES-B	yes	no	R_{DIC}	standard
PISCES-C	yes	yes	$R_{CO2(aq)}$	standard
PISCES-D	yes	yes	R_{DIC}	less southern ocean ventilation
PISCES-E	no	no	R_{DIC}	standard

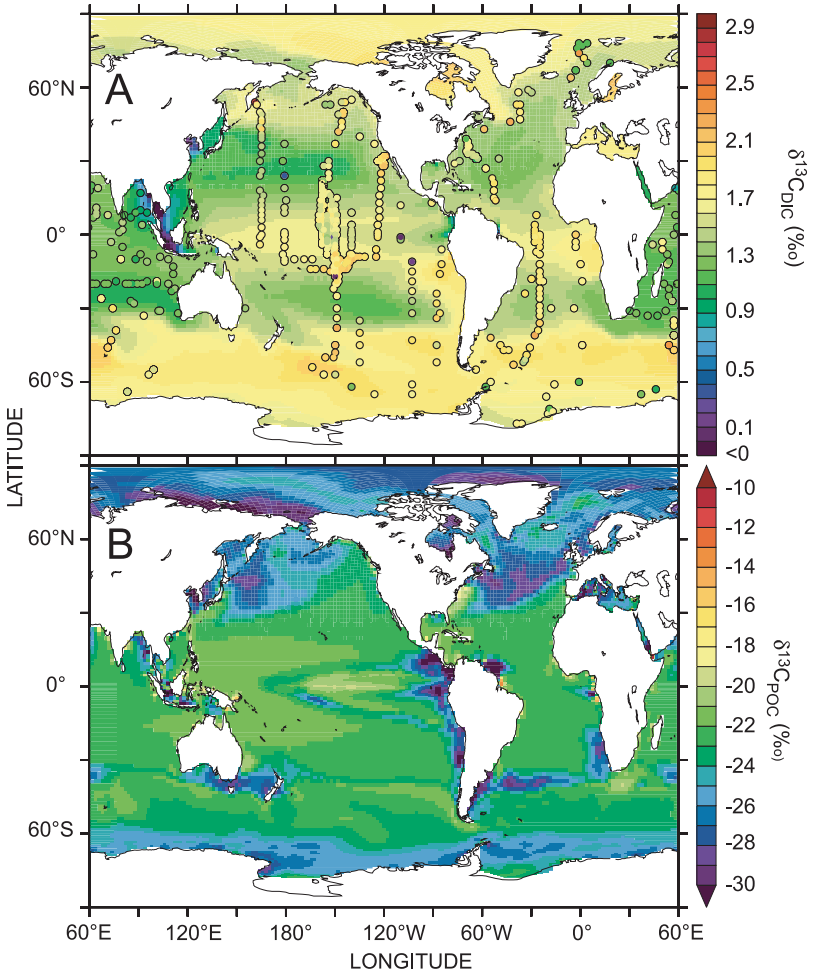

Figure 2. (a) The annually averaged distribution of $\delta^{13}C_{DIC}$ (‰) in surface waters versus the compendium of observations published by *Gruber et al.* [1999] and (b) the annually averaged distribution of $\delta^{13}C_{POC}$ (‰) in surface waters from PISCES-A.

to consider that deep water also contains an older (i.e., heavier) $\delta^{13}C_{DIC}$ signal from the atmosphere. Therefore fractionation during primary productivity [*Gruber et al.*, 1999] and the upwelling of older water, as well as the influx of atmospheric $^{13}CO_2$ will contribute to the $\delta^{13}C_{DIC}$ gradient downstream of upwelling zones (e.g., the Peru and Benguela upwelling zones, Figure 2a). On the other hand, low $\delta^{13}C_{DIC}$ values in subtropical gyres reflect both temperature dependent fractionation during gas exchange [*Gruber et al.*, 1999], as well as the increased overall invasion of isotopically light atmospheric CO_2.

[16] Predictions of $\delta^{13}C_{POC}$ from PISCES-A (Figure 2b) reflect the major trends in measured $\delta^{13}C_{POC}$ well. Overall, the majority of the global ocean displays a $\delta^{13}C_{POC}$ of around −21 to −22‰ and declines in regions typified by substantial phytoplankton growth (e.g., the North Atlantic, Figures 2b, 4c and 4d). Between the sub-Antarctic and Antarctic regions of the Southern Ocean we predict a decline in $\delta^{13}C_{POC}$ from −21 to −30‰ (Figure 2b), which corresponds well with measured changes of −20 to −30‰ [*Dehairs et al.*, 1997; *Popp et al.*, 1999; *O'Leary et al.*, 2001]. This is related to both an increase in CO_2(aq) concentrations in colder waters, which elevates ε_p, as well as greater total primary production near the Antarctic shelf. In the North Pacific, our predictions of between −24 and −28‰ (Figure 2b) compare well with observations of −23.5 to −26.6‰ [*Guo et al.*, 2004; *Chen et al.*, 2006]. The "heaviest' POC is predicted to be found at low latitudes (especially in the western subtropical Pacific, Figures 2b, 4b and 4c) and is due to the decline in ε_p that results from the lower CO_2(aq) concentrations and high phytoplankton growth rates that prevail in warm surface waters. Overall, we find that $\delta^{13}C_{POC}$ shows a high degree of absolute variability within both the Atlantic and Pacific Ocean basins (Figures 4c and 4d represent the total model variability in space and time), which is related to spatiotemporal heterogeneity in CO_2(aq), phytoplankton growth rates and biological production that is induced by ocean mixing.

3.2. Controls on the Deep Ocean $\delta^{13}C_{DIC}$

[17] While we accurately represent the decline in deep $\delta^{13}C_{DIC}$ from the Atlantic to Pacific deep ocean basins,

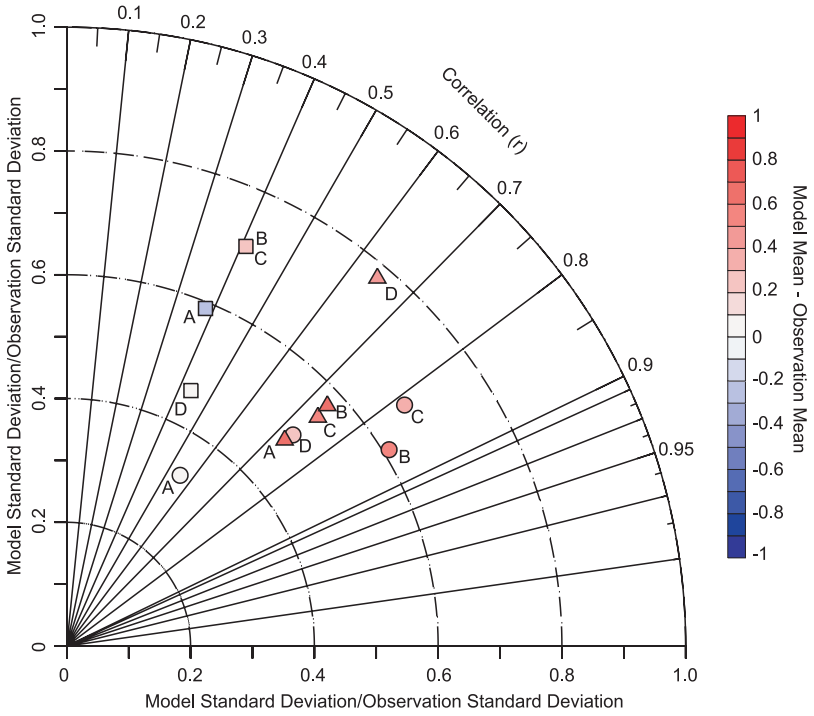

Figure 3. A Taylor plot of PISCES-A (A), PISCES-C (C) and PISCES-D (D) relative to observations of *Gruber et al.* [1999] between 0 and 5500 m (circles), 0 to 10 m (squares) and 1000 to 5500 m (triangles), as a function of the correlation coefficient (r) and the normalized standard deviation (model standard deviation/observations standard deviation), as well as the model mean−observations mean (‰). See Table 1 for a description of the different models. For reference, a perfect simulation would display a correlation coefficient of 1 and a normalized standard deviation of 1.

values are consistently ∼0.4 ‰ too high during PISCES-A (Figure 3, Figure 5a, and Table 2). Although the deep ocean $\delta^{13}C_{DIC}$ is driven to low values by the remineralization of isotopically light POC that sinks from surface waters, mixing with the high $\delta^{13}C_{DIC}$ of ocean surface waters subsequently increases the deep $\delta^{13}C_{DIC}$. The fact that the degree of mismatch between PISCES-A and observations is greatest in the Southern and Pacific Oceans (Figure 5a)

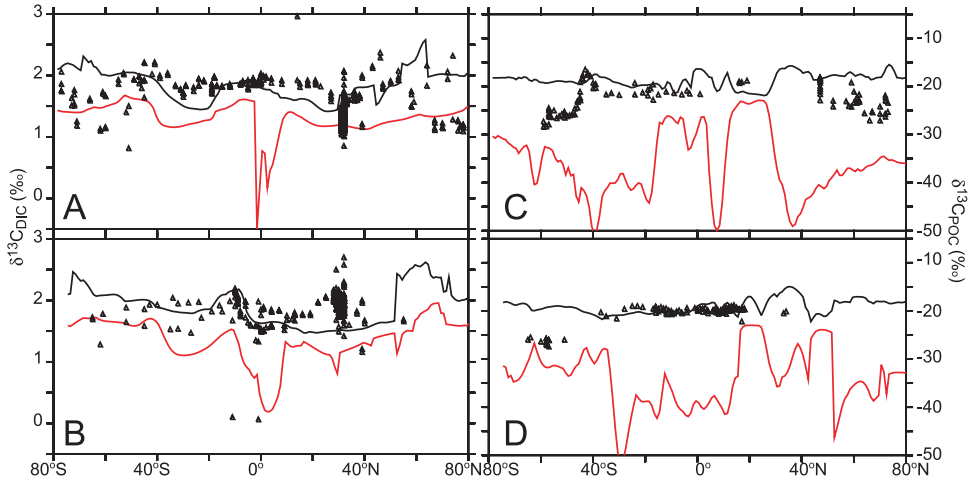

Figure 4. The absolute (zonal and temporal) maximum (black line) and minimum (red line) $\delta^{13}C_{DIC}$ (‰) and $\delta^{13}C_{POC}$ (‰) in surface waters in 1990 for the Atlantic (70°E to 20°W, panels a and c, respectively) and Pacific (70°E to 140°E, panels b and d, respectively) Ocean basins from PISCES-A. In panels a and b, we include the $\delta^{13}C_{DIC}$ data from *Gruber et al.* [1999], whereas in panels c and d, we include the data from *Goericke and Fry* [1994].

Table 2. A Summary of the Observational and Model $\delta^{13}C_{DIC}$ Statistics Over a Variety of Depth Ranges (Illustrated in Figure 3)[a]

	Data	PISCES-A	PISCES-B	PISCES-C	PISCES-D
			0–5500m		
Mean, ‰	1.252	1.345	1.781	1.630	1.534
St. Dev., ‰	0.61	0.202	0.372	0.409	0.305
Correlation	-	0.553	0.855	0.814	0.731
			0–10m		
Mean, ‰	1.587	1.349	1.970	1.820	1.651
St. Dev., ‰	0.390	0.230	0.162	0.276	0.179
Correlation	-	0.380	0.422	0.409	0.437
			1000–5500m		
Mean, ‰	0.548	1.198	1.230	1.104	1.001
St. Dev., ‰	0.419	0.203	0.240	0.230	0.326
Correlation		0.727	0.735	0.739	0.645

[a]The model experiments are summarized in Table 1.

suggests that deep water production near Antarctica might be important. This can be illustrated by examining the column inventory of CFC-11, which accumulates from the atmosphere and reflects the degree of ocean ventilation [e.g., *Dutay et al.*, 2002]. PISCES-A uses an ocean circulation that has a high degree of deep water ventilation near the Antarctic continental shelf (Figures 6a and 6b), an important region of deep water formation for the deep Southern and Pacific Ocean basins. Increased mixing with high $\delta^{13}C_{DIC}$ surface waters therefore results in elevated $\delta^{13}C_{DIC}$ values throughout the deep Southern and Pacific Oceans, relative to observations (Figure 5a).

[18] By using an alternative representation of oceanic circulation that exhibits less Antarctic continental shelf ventilation (PISCES-D, Figure 6c), we find that the deep ocean $\delta^{13}C_{DIC}$ declines by 0.4 to 0.7‰ and by 0.3 to 0.4‰ throughout the Southern and Pacific Ocean basins, respectively, in an altogether better agreement with observations (Figures 3, 5b, and Table 2). In contrast, values of $\delta^{13}C_{DIC}$ in the deep Atlantic Ocean change little (Figure 5b). Additionally, PISCES-D also manages to better represent the observed variability in deep $\delta^{13}C_{DIC}$, as illustrated by the increased normalized standard deviation (relative to PISCES-A, Figure 3, Table 2). Therefore the degree of deep water ventilation that occurs near the Antarctic conti-

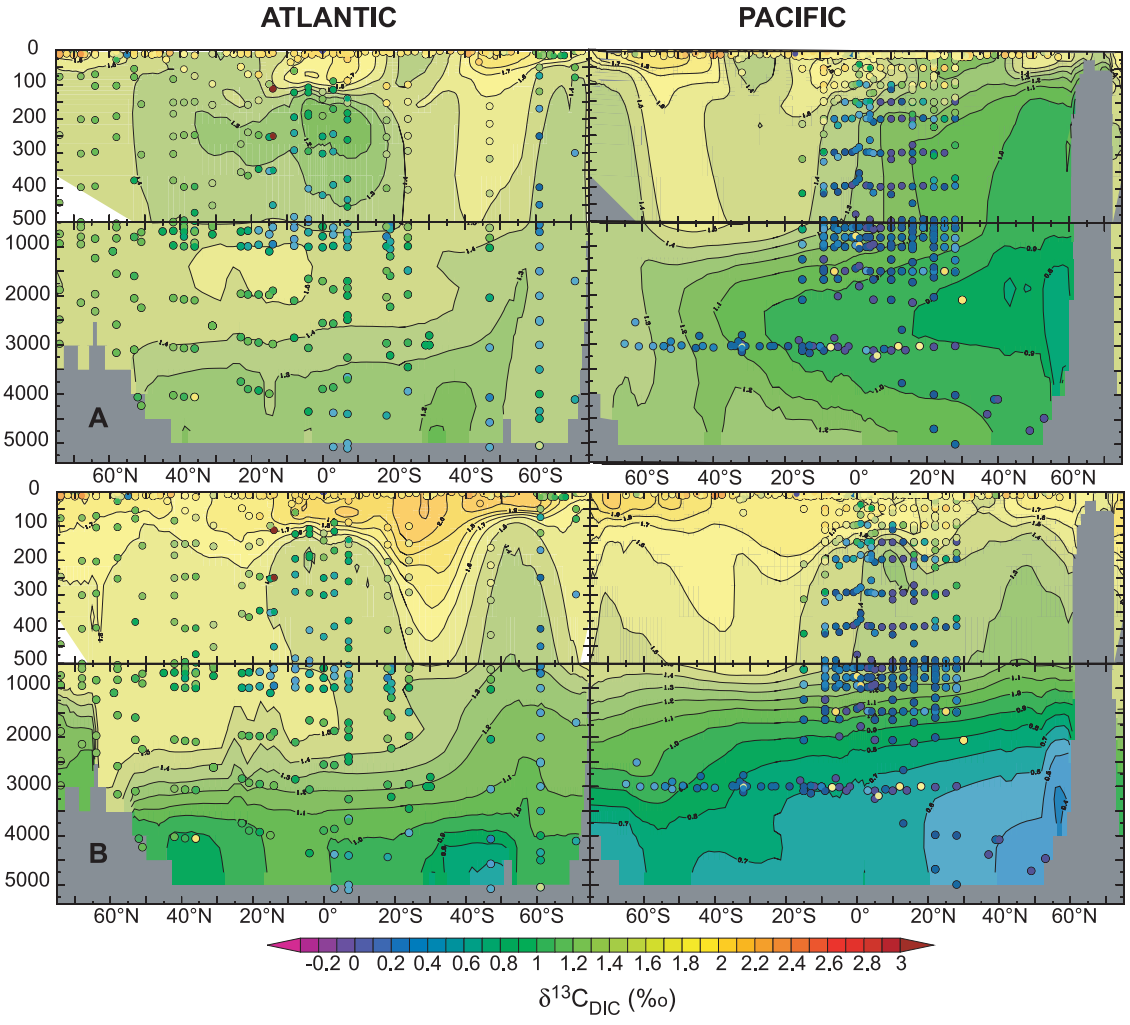

Figure 5. The annually averaged latitude-depth distribution of $\delta^{13}C_{DIC}$ (‰) versus the compendium of observations published by *Gruber et al.* [1999]; (a) the standard model circulation (PISCES-A) and (b) an alternative representation of ocean circulation (PISCES-D, see Figure 6).

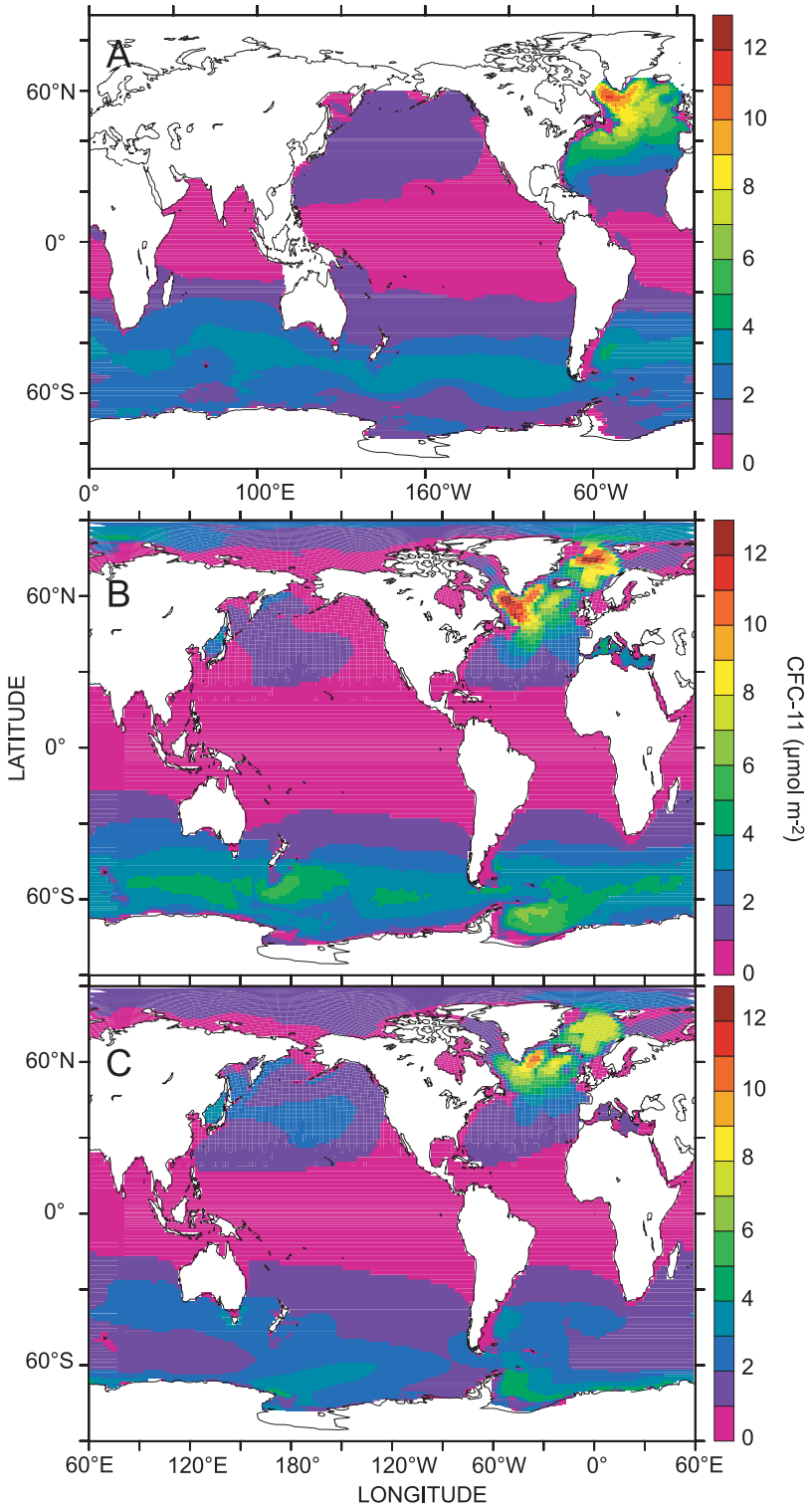

Figure 6. The 1991 depth integrated inventory of CFC-11 (μmol m^{-2}) from (a) the GLODAP database, (b) our standard circulation (PISCES-A) and (c) an alternative representation of ocean circulation (PISCES-D).

nental shelf is critical in modifying the deep ocean $\delta^{13}C_{DIC}$ distribution that initially arises from the sinking and remineralization of POC. In addition, biological processes (such as fractionation during photosynthesis and respiration of organic matter) are of importance in setting the surface and deep end-member $\delta^{13}C_{DIC}$. Finally, the timescales of atmospheric isotopic equilibration, fractionation during photo-

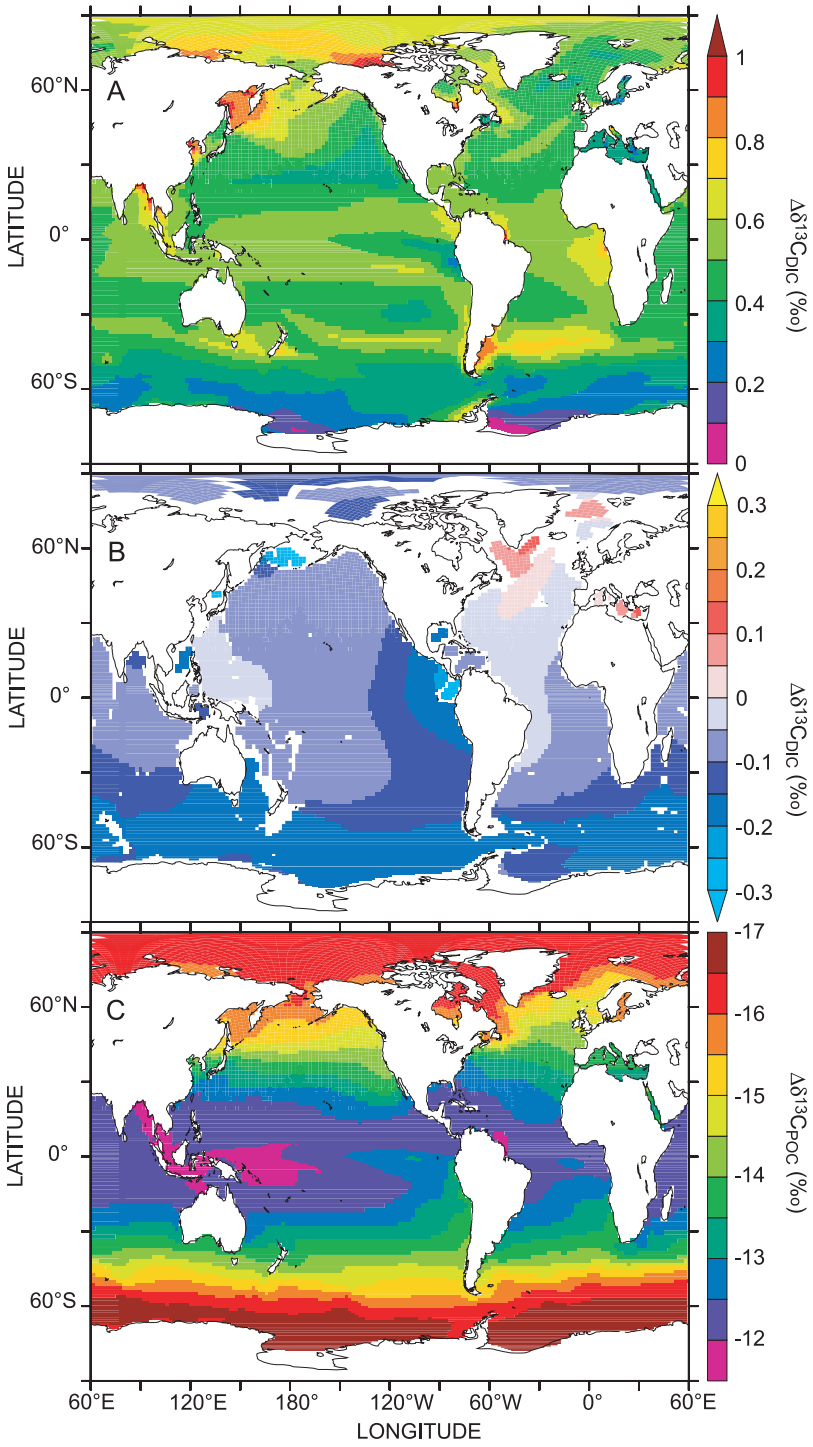

Figure 7. The change in (a) $\delta^{13}C_{DIC}$ (‰) at the surface, (b) $\delta^{13}C_{DIC}$ at 2500 m (‰), and (c) $\delta^{13}C_{POC}$ at the surface (‰) during PISCES-C, relative to PISCES-A, when phytoplankton are assumed to transport only CO_2(aq).

synthesis, and downwelling will constrain the relative influence of atmospheric $\delta^{13}CO_2$ on the deep ocean $\delta^{13}C_{DIC}$.

[19] Overall, it is clear that a multitude of processes, both physical (ocean ventilation and surface $\delta^{13}C_{DIC}$ near the Antarctic continental shelf, atmospheric equilibration) and biological (variability in ε_p that is a function of CO_2(aq), μ and species composition), ultimately control the deep ocean $\delta^{13}C_{DIC}$. Of these, changes in ocean ventilation herald the largest variation in $\delta^{13}C_{DIC}$, highlighting the potential for physical processes to control the reduction in deep ocean

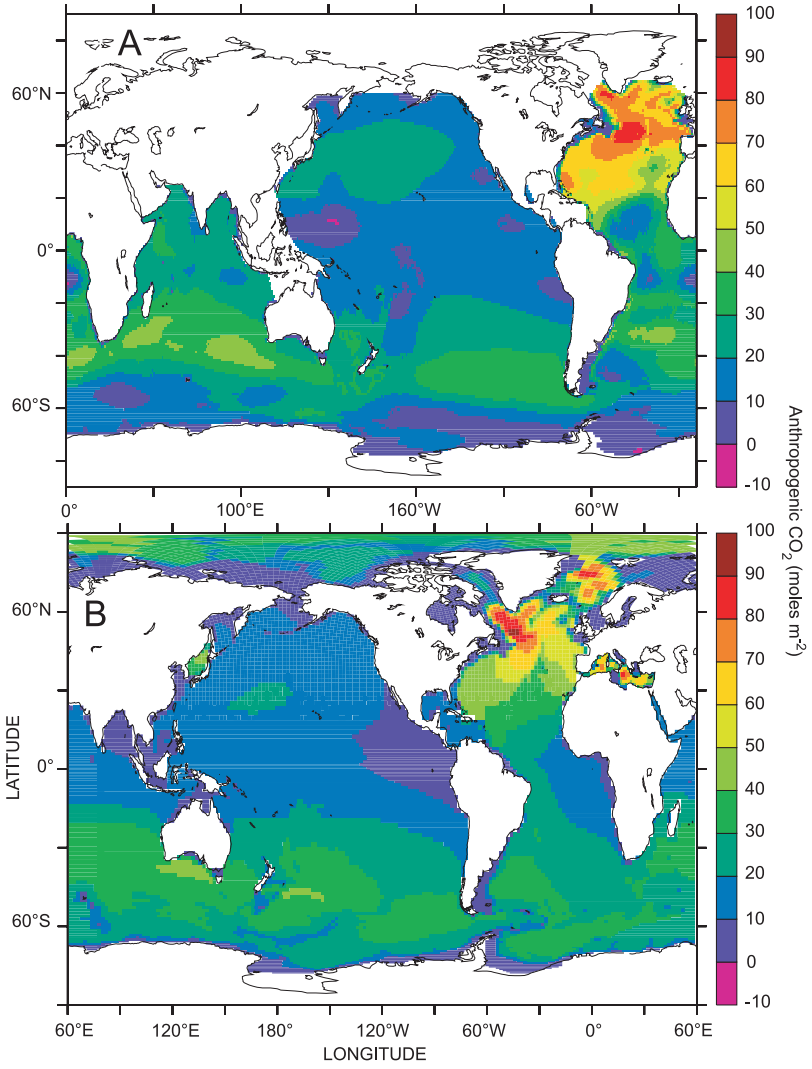

Figure 8. The accumulation of anthropogenic CO_2 (moles m^{-2}) from (a) *Sabine et al.* [2004] and (b) PISCES-A.

$\delta^{13}C_{DIC}$ that occurred at the Last Glacial Maximum (LGM) [sensu *Toggweiler*, 1999]. In this sense, reduced ocean ventilation at the LGM [e.g., *Lynch-Stieglitz et al.*, 2007] might amplify the response of deep ocean $\delta^{13}C_{DIC}$ to any decline that might have arisen from an increase in surface primary production.

3.3. Mode of Inorganic C Access

[20] Although surface $\delta^{13}C_{DIC}$ increases if we assume that phytoplankton only transport CO_2(aq) during photosynthesis, deep values are relatively unmodified. The $\delta^{13}C_{DIC}$ of surface waters increases by around 0.4 to 0.5‰ at low latitudes and by as much as 1‰ in productive high latitude regions during PISCES-C (Figure 7a). Nevertheless, at depth, $\delta^{13}C_{DIC}$ changes little (±0.2‰, Figure 3, Figure 7b, and Table 2), suggesting that deep distributions of $\delta^{13}C_{DIC}$ might be relatively insensitive to changes surface fractionation. As outlined above, although the remineralization of light POC will reduce deep ocean $\delta^{13}C_{DIC}$, mixing with the (now higher) $\delta^{13}C_{DIC}$ of surface waters dilutes much of the change at depth. Relative to observations, we end up overestimating surface $\delta^{13}C_{DIC}$ by around 0.6‰ during PISCES-C, but the representation of the observed seasonal variability improves (Figure 3 and Table 2). The better representation of surface $\delta^{13}C_{DIC}$ during PISCES-A may also be due to the overestimation of deep $\delta^{13}C_{DIC}$ during these simulations (Figure 5a and Table 2), which can mix into surface waters.

[21] Despite a potentially better fit to the $\delta^{13}C_{DIC}$ data, $\delta^{13}C_{POC}$ declines dramatically if phytoplankton are assumed to only transport CO_2(aq) during photosynthesis. In surface waters, $\delta^{13}C_{POC}$ is reduced by 17 and 12‰ between high and low latitudes, respectively (Figure 7c). For reference, this would reduce Southern Ocean and Equatorial Atlantic $\delta^{13}C_{POC}$ to <-45 and -30 ‰, respectively, well beyond observations of between -16 and -36 ‰ [e.g., *Goericke and Fry*, 1994]. This is because $R_{CO2(aq)}$ is always less than R_{DIC} during PISCES-C and phytoplankton therefore accu-

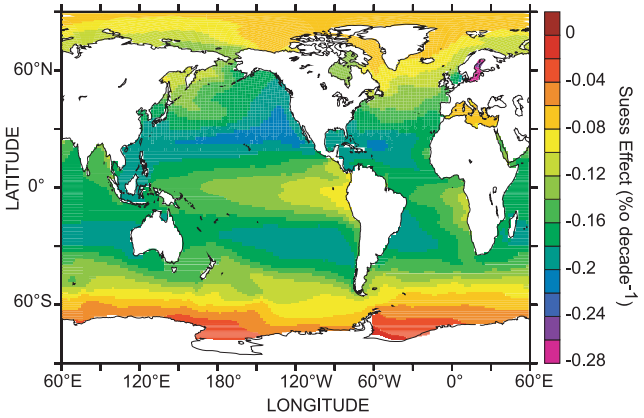

Figure 9. The surface ocean ^{13}C Suess effect (‰ decade^{-1}) during PISCES-A between 1970 and 2000.

mulate less ^{13}C (for a given rate of C fixation). However, this sensitivity will be related to the parameterization of ε_p (equation (1)), which was determined in equatorial Pacific [*Laws et al.*, 1995]. Nevertheless, ε_p is around 20–22‰ and 18‰ in the Southern Ocean and equatorial Pacific, respectively (during PISCES-A) and compares well to observations of >20‰ in the Southern Ocean [*Popp et al.*, 1999] and 16‰ in the equatorial Pacific [*Bidigare et al.*, 1999]. Indeed, recent field observations in both the Southern Ocean and sub Arctic Pacific have found that between 50 and 90% of total phytoplankton DIC uptake was associated with direct HCO_3^- uptake, rather than CO_2(aq) [*Cassar et al.*, 2004; *Tortell et al.*, 2006]. Accordingly, for our predictions of $\delta^{13}C_{POC}$ to remain within the observational range we must assume that phytoplankton are not solely reliant on CO_2(aq) for photosynthesis. In reality, it is likely that a range of strategies exist, that are driven by local conditions or perhaps species specific inorganic C transport mechanisms [e.g., *Raven and Johnston*, 1991].

3.4. Overall Response to Changes in Atmospheric pCO_2 Between 1860 and 2000

[22] Globally, our results compare well to a recent data-based calculation of the oceanic sink for atmospheric CO_2 over the past 194 years. *Sabine et al.* [2004] used inorganic C measurements, alongside a tracer separation technique, to estimate the global ocean CO_2 sink to be 118 ± 19 Pg C (between 1800 and 1994) and we find the ocean sink to be 93.65 Pg C over our shorter study period (between 1860 and 1994). Spatially, our results exhibit maximal C_{ant} column inventories in regions typified by deep ventilation (Figure 6b and Figure 8b), primarily the north Atlantic, but also the Southern Ocean (e.g., around 40°S), in agreement with the estimates of *Sabine et al.* [2004] (Figure 8a). The mean ocean sink for CO_2 in the 1990s is 1.86 Pg C a^{-1} and increases by 0.31 Pg C a^{-1} between the 1980s and the 1990s. This agrees well with the recent Intergovernmental Panel on Climate Change (IPCC) report, which estimates (using a variety of techniques) a mean ocean sink of 1.8 ± 0.8 and 2.2 ± 0.4 Pg C a^{-1} during the 1980s and 1990s, respectively [*IPCC*, 2007].

3.5. The Ocean ^{13}C Suess Effect

[23] Both the increased total flux of CO_2 from the atmosphere to the ocean, as well as the reduction in $\delta^{13}CO_2$, and gas exchange fractionation contributes to the rate of change in $\delta^{13}C_{DIC}$ (defined hereafter as the ocean ^{13}C Suess effect) since 1860. We find the ^{13}C Suess effect between 1860 and 2000 to be −0.07‰ decade^{-1} and increases to −0.18‰ decade^{-1} between 1970 and 2000 (a 2.6 fold increase). Observed changes in ocean $\delta^{13}C_{DIC}$ of −0.15 and −0.171 ‰ decade^{-1} between 1970 and 1990 [*Bacastow et al.*, 1996 and *Sonnerup et al.*, 1999, respectively] are in good agreement with our global estimate of −0.174‰ decade^{-1} for the same time period. We find that the ocean ^{13}C Suess effect is always approximately 65% of the change in atmospheric $\delta^{13}CO_2$ (0.11 and 0.27 ‰ decade^{-1} for 1860–2000 and 1970–2000, respectively), regardless of the time increment over which it is evaluated. This compares well with previous estimates of between 60 and 70% [*Keeling*, 1979; *Broecker and Peng*, 1993] and reflects longer equilibration time for ^{13}C in the ocean, relative to the atmosphere. The change in atmospheric pCO_2 alone (PISCES-B) contributes as little as 15% (−0.011‰ decade^{-1}) to the overall ^{13}C Suess effect between 1860 and 2000. Consequently, despite the importance of the total flux of CO_2 and, to a lesser degree, temperature-dependent fractionation, the vast majority of the documented reduction in ocean $\delta^{13}C_{DIC}$ results from the dramatic decline in atmospheric $\delta^{13}CO_2$ (Figure 1).

[24] The ocean ^{13}C Suess effect displays a wide degree of spatial variability in surface waters, varying from almost 0 to < −0.24‰ decade^{-1} between 1970 and 2000 (Figure 9). This corresponds well with basin estimates of −0.18, −0.18, and −0.14 ‰ decade^{-1} in the Atlantic [*Quay et al.*, 2007], Pacific [*Quay et al.*, 2003], and Indian [*Sonnerup et al.*, 2000] Oceans, respectively, as well as the poleward decline along 140°E in the Southern Ocean (from −0.16 to 0.06 ‰ decade^{-1}) noted by *McNeil et al.* [2001] (Figure 9). Overall, the largest reductions in $\delta^{13}C_{DIC}$ occur in the sub tropical gyres, with a marked decline in the ^{13}C Suess effect at high latitudes and near tropical upwellings (especially in the Pacific, Figure 9).

[25] Understanding the spatial distribution of the ^{13}C Suess effect necessitates a consideration of ocean mixing and circulation. In particular, upwelling of higher $\delta^{13}C_{DIC}$ (i.e., older) deep waters dilutes the surface ^{13}C Suess effect (in the Eastern Pacific, for example, Figure 9), as well as minimizing the exposure of surface waters for the uptake of atmospheric CO_2 and isotopic equilibration. Alternatively, in regions typified by little deep water ventilation (such as sub-tropical gyres) surface waters have a longer residence time and thus exhibit the greatest reductions in $\delta^{13}C_{DIC}$ (Figure 9). In the Southern Ocean, both the temperature dependent fractionation between CO_2(aq) and DIC that follows gas exchange and surface water subduction prior to isotopic equilibrium reduces the ^{13}C Suess effect (Figure 9) [*McNeil et al.*, 2001]. At the Bermuda Atlantic Time Series (BATS, ∼30°N in Figure 4) and Hawaii Ocean Time Series (HOT, around 25°N in Figure 4) we only account for around half of the observed $\Delta\delta^{13}C_{DIC}$ of −0.025 ‰ a^{-1} [*Gruber et al.*, 1999]. This is most likely

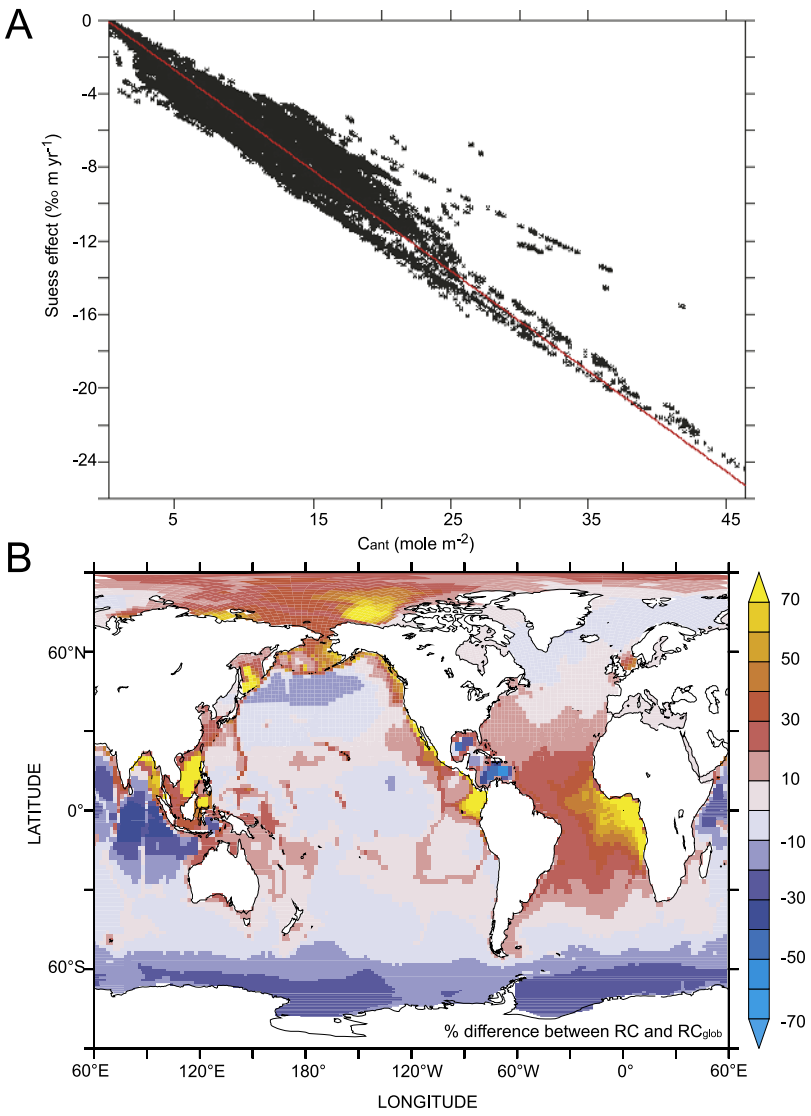

Figure 10. (a) The relationship between depth integrated anthropogenic carbon (C_{ant}, mole m^{-2}) and the depth integrated Suess effect (‰ m a^{-1}) between 1970 and 2000, with the global average RC (RC_{glob}, defined as $\Delta\delta^{13}C_{DIC}/C_{ant}$) represented by a red line. (b) A spatial representation of the percentage difference in RC, relative to RC_{glob}.

due to the low resolution of our global model, relative to the individual ocean stations concerned, the absence of any interannual changes in circulation and, for BATS in particular, an under estimate of C_{ant} in the western subtropical Atlantic (Figure 8).

3.6. Relating the Ocean Suess Effect to the Accumulation of Anthropogenic Carbon

[26] As $\Delta\delta^{13}C_{DIC}$ is often used to derive ocean uptake of C_{ant}, it is of interest to examine the simulated relationship between the accumulation of C_{ant} and the $\Delta\delta^{13}C_{DIC}$. The Suess effect can be related to C_{ant} via the parameter 'RC' (defined as: $\Delta\delta^{13}C_{DIC}/\Delta DIC$, *McNeil et al.* [2001]). Between 1970 and 2000, we find a good relationship between depth integrated $\Delta\delta^{13}C_{DIC}$ (‰ m yr^{-1}) and C_{ant} (mole m^{-2}) (Figure 10a) and derive a global average RC (RC_{glob}) of -0.0164 ‰ (μmol kg^{-1})$^{-1}$. While RC_{glob} is similar to the global "dynamic constraint' of between -0.016 and -0.019‰ (μmol kg^{-1})$^{-1}$ proposed by *Heimann and Maier-Reimer* [1996], we caution against applying RC_{glob} to sparse regional $\Delta\delta^{13}C_{DIC}$ observations, as RC varies by as much as ±70% locally (relative to RC_{glob}, Figure 10b, as well as *Heimann and Maier-Reimer* [1996]). Accordingly, RC has been observed to decline poleward from -0.015 to -0.007‰ (μmol kg^{-1})$^{-1}$ in the Southern Ocean [*McNeil et al.*, 2001] and we confirm that applying RC_{glob} would underestimate C_{ant} by 10 to 30% (Figure 10b). As the subduction of cold surface waters decouples $\Delta\delta^{13}C_{DIC}$ from ΔDIC, only a small change in $\delta^{13}C_{DIC}$ accompanies the accumulation of C_{ant} (i.e., a low RC). In fact, the shallower penetration of $\Delta\delta^{13}C_{DIC}$, relative to C_{ant}, that was observed by *McNeil et al.* [2001] along 140°E appears to be a consistent feature of the Antarctic region of

the Southern Ocean (Figure 10b), suggesting RC_{glob} cannot derive C_{ant} in this important ocean region. While RC is almost equal to RC_{glob} in the high North Atlantic, it increases sharply south of ~40°N (to up to 0.028 ‰ (μmol kg^{-1})$^{-1}$, Figure 10b), which is in accord with observations of −0.024‰ (μmol kg^{-1})$^{-1}$ (or 50% greater than our RC_{glob}) by *Kortzinger et al.* [2003]. In the central Pacific, RC remains within ±10% of RC_{glob}, although we note higher values near HOT and the equatorial upwelling (Figure 10b).

[27] While quantitatively less important than the invasion of isotopically light C_{ant}, increased biotic fractionation can also play a role in controlling the measured Suess effect. As the ocean DIC inventory increases, the greater concentration of CO_2(aq) permits greater biotic fractionation against ^{13}DIC [e.g., *Laws et al.*, 1995, 1997]. Accordingly, ε_p increased by an average of 0.25 ‰, or 0.018‰ decade^{-1}, relative to the overall Suess effect of −0.07‰ decade^{-1} (between 1860 and 2000, during PISCES-A) in surface waters. We suggest that the observed Suess effect ($\Delta\delta^{13}C_{DICobs}$) will reflect contributions from the invasion of C_{ant} ($\Delta\delta^{13}C_{DICatm}$), as well as changes in biotic fractionation ($\Delta\delta^{13}C_{DICbio}$) and ocean circulation ($\Delta\delta^{13}C_{DICcirc}$). As there was no change in ocean circulation during our simulations (i.e., $\Delta\delta^{13}C_{DICcirc} = 0$), the Suess effect associated with the uptake of C_{ant} ($\Delta\delta^{13}C_{DICatm}$) can be approximated to be −0.088 ‰ decade^{-1} (26% greater than $\Delta\delta^{13}C_{DICobs}$). This would suggest that unless $\Delta\delta^{13}C_{DICcirc}$ and $\Delta\delta^{13}C_{DICbio}$ can be accounted for, any estimate of C_{ant} that is based on $\Delta\delta^{13}C_{DICobs}$ will be conservative.

4. Perspectives

[28] In terms of understanding the ocean $\Delta\delta^{13}C_{DIC}$ and the uptake of C_{ant}, our prognostic ^{13}C parameterization results in a similar RC_{glob} to previous models [e.g., *Heimann and Maier-Reimer*, 1996], but also permits us to better represent the observed regional heterogeneity in RC, especially in the Southern Ocean (Figure 10b). This is because earlier generation ocean models [e.g., *Heimann and Maier-Reimer*, 1996] utilized much longer timesteps (one month versus a few hours) and coarser vertical and horizontal resolution. Moreover, in the future this model configuration will be used to investigate changes in ocean δ^{13}C that result from future or past changes in climate, as well as atmospheric pCO_2 and $\delta^{13}CO_2$. In doing so, it will be possible to address the impact on ocean δ^{13}C of the variability in phytoplankton fractionation that results from changes in growth rate, and species composition (as estimated for [CO_2(aq)] here) that are mediated by ocean circulation and/or exogenous nutrient delivery. For example, since dust deposition of iron is postulated to have been greater at the LGM, we would anticipate a concomitant decline in phytoplankton fractionation as growth rates increase and large diatoms replace smaller nanophytoplankton would reduce surface $\delta^{13}C_{DIC}$. It is currently unclear how such processes will interact with the physically driven changes in the ocean δ^{13}C at the LGM [e.g., *Lynch-Stieglitz et al.*, 2007]. On the other hand, the future ocean will be warmer (ostensibly reducing δ^{13}C via gas exchange fractionation) and will also display greater surface stratification [e.g., *Sarmiento et al.*, 2004]. Reduced vertical mixing should elevate δ^{13}C (via reduced mixing with light deeper waters), but will also increase phytoplankton fractionation due to the change in growth rate and species composition that results from lesser vertical nutrient supply [e.g., *Bopp et al.*, 2005]. Our model can therefore be used to better constrain the relative contributions of changes in ocean circulation ($\Delta\delta^{13}C_{DICcirc}$) and biological productivity ($\Delta\delta^{13}C_{DICbio}$), as well as uptake of anthropogenic carbon ($\Delta\delta^{13}C_{DICatm}$), to the measured ocean ^{13}C Suess effect ($\Delta\delta^{13}C_{DICobs}$).

5. Conclusions

[29] In general, biological and chemical fractionation processes will dictate the initial surface and deep patterns in $\delta^{13}C_{DIC}$ that are modified by ocean mixing. Elevated surface $\delta^{13}C_{DIC}$ values will be found in regions of high primary production or cold temperatures, while deep $\delta^{13}C_{DIC}$ will be reduced underneath zones of significant export flux, as well as along the deep ocean conveyor belt (via the remineralization of isotopically light POC). However, the ocean system is dynamic and the value of $\delta^{13}C_{DIC}$ in a given space and time is also controlled by physical mixing. High rates of ventilation will reduce and increase the surface and deep $\delta^{13}C_{DIC}$, respectively (by as much as 0.7‰), as a function of the surface and deep end-members. While the ^{13}C Suess effect is a first order function of the atmospheric $\delta^{13}CO_2$ and overall C flux, the spatial distributions are also controlled by ocean ventilation and the degree isotopic equilibrium with the atmosphere. Accordingly, while we confirm a tight relationship between the depth-integrated Suess effect and anthropogenic carbon globally, there is a large degree of regional heterogeneity in RC (±60%) that should be considered when deriving the accumulation of C_{ant} from local observations. In addition, the overall Suess effect reflects contributions from anthropogenic carbon, biotic processes (such as changes in fractionation) and ocean circulation. Including ^{13}C in a state of the art ocean-biogeochemical model will permit the future appraisal as to the impact of biological variability in fractionation on ocean δ^{13}C that is driven by future or past variability in circulation and/or exogenous nutrient inputs.

[30] **Acknowledgments.** We thank Nicolas Cassar, Niki Gruber, and two anonymous reviewers for their insightful comments on our manuscript. Funding was provided by the project ANR-GOBAC and all simulations were performed at the French National computing center IDRIS. This is LSCE contribution number 2907.

References

Aumont, O., and L. Bopp (2006), Globalizing results from ocean in situ iron fertilization studies, *Global Biogeochem. Cycles*, *20*, GB2017, doi:10.1029/2005GB002591.

Bacastow, R., C. D. Keeling, T. J. Lueker, M. Wahlen, and W. G. Mook (1996), The ^{13}C Suess effect in the world surface oceans and its implications for oceanic uptake of CO2: Analysis of observations at Bermuda, *Global Biogeochem. Cycles*, *10*, 335–346.

Bidigare, R. R., K. L. Hanson, and K. O. Buessler (1999), Iron stimulated changes in C-13 fractionation and export by equatorial Pacific phytoplankton: Toward a paleogrowth rate proxy, *Paleoceanography*, *14*, 589–595.

Bopp, L., O. Aumont, P. Cadule, S. Alvain, and M. Gehlen (2005), Response of diatoms distribution to global warming and potential implications: A global model study, *Geophys. Res. Lett.*, *32*, L19606, doi:10.1029/2005GL023653.

Broecker, W. S., and T. H. Peng (1993), Evaluation of the ^{13}C constraint on the uptake of fossil fuel CO2 by the ocean, *Global Biogeochem. Cycles*, *7*, 619–626.

Burkhardt, S., U. Riesebell, and I. Zondervan (1999), Effect of growth rate, CO2 concentration, and cell size on the stable carbon isotope fractionation in marine phytoplankton, *Geochim. Cosmochim. Acta*, *63*, 3729–3741.

Cassar, N., E. A. Laws, R. R. Bidigare, and B. N. Popp (2004), Bicarbonate uptake by Southern Ocean phytoplankton, *Global Biogeochem. Cycles*, *18*, GB2003, doi:10.1029/2003GB002116.

Chen, M., L. Guo, Q. Ma, Y. Qiu, R. Zhang, E. Lv, and Y. Huang (2006), Zonal patterns of $\delta^{13}C$, $\delta^{15}N$ and 210Po in the tropical and subtropical North Pacific, *Geophys. Res. Lett.*, *33*, L04609, doi:10.1029/2005GL025186.

Ciais, P., et al. (1995), Paritioning of ocean and land uptake of CO2 as inferred by $\delta^{13}C$ measurements from the NOAA climate monitoring and diagnostics laboratory global air sampling network, *J. Geophys. Res.*, *100*, 5051–5070.

Dehairs, F., E. Kopczynska, P. Nielsen, C. Lancelot, D. Bakker, W. Koeve, and L. Goeyens (1997), ^{13}C of Southern Ocean suspended matter during spring and early summer: Regional and temporal variability, *Deep Sea Res., Part II*, *44*, 129–142.

Dutay, J.-C., et al. (2002), Evaluation of ocean model ventilation with CFC-11: Comparison of 13 global ocean models, *Ocean Modell.*, *4*, 89–120.

Farquhar, G. D., M. H. O'Leary, and J. A. Barry (1982), On the relationship between carbon isotopic discrimination and the intercellular concentration carbon dioxide concentration in leaves, *Aust. J. Plant Physiol.*, *9*, 121–137.

Francey, R. J., et al. (1999), A 1000-year high precision record of $\delta^{13}C$ in atmospheric CO_2, *Tellus B*, *51*, 170.

Goericke, R., and B. Fry (1994), Variations of marine plankton $\delta^{13}C$ with latitude, temperature and dissolved CO2 in the world ocean, *Global Biogeochem. Cycles*, *8*, 85–90.

Guo, L., T. Tanaka, D. Wang, N. Tanaka, and A. Murata (2004), Distributions, speciation and stable isotope composition of organic matter in the southeastern Bering Sea, *Mar. Chem.*, *91*, 211–226.

Gruber, N., and C. D. Keeling (2001), An improved estimate of the isotopic air-sea disequilibrium of CO2: Implications for the oceanic uptake of anthropogenic CO2, *Geophys. Res. Lett.*, *28*, 555–558.

Gruber, N., C. D. Keeling, R. B. Bacastow, P. R. Guenther, T. J. Leuker, M. Wahlen, H. A. J. Meijer, W. G. Mook, and T. F. Stocker (1999), Spatiotemporal patterns of carbon-13 in the global surface oceans and the oceanic Suess effect, *Global Biogeochem. Cycles*, *13*, 307–335.

Heimann, M., and E. Maier-Reimer (1996), On the relations between the oceanic uptake of CO2 and its carbon isotopes, *Global Biogeochem. Cycles*, *10*, 89–110.

IPCC (2007), The Physical Science Basis. *Contribution of Working Group I to the Fourth Assessment Report of the Intergovernmental Panel on Climate Change*. S. Solomon, D. Qin, M. Manning, Z. Chen, M. Marquis, K. B. Averyt, M. Tignor, and H. L. Miller, Eds. (2007), Cambridge University Press, NY, USA. 996 pp.

Keeling, C. D. (1979), The Suess Effect: ^{13}Carbon and ^{12}Carbon interations, in *Environment International*, *2*, 229–300, Pergamon, Tarrytown, N. Y.

Keeling, C. D., S. C. Piper, R. B. Bacastow, M. Wahlen, T. P. Whorf, M. Heimann, and H. A. Meijer (2001), Exchanges of Atmospheric CO2 and $CO^{13}CO2$ with the Terrestrial Biosphere and Oceans from 1978 to 2000. I Global Aspects. SIO Reference No. 01–06.

Kortzinger, A., P. D. Quay, and R. E. Sonnerup (2003), Relationship between anthropogenic CO2 and the 13C Suess effect in the North Atlantic Ocean, *Global Biogeochem. Cycles*, *17*(1), 1005, doi:10.1029/2001GB001427.

Laws, E. A., B. N. Popp, R. R. Bidigare, M. C. Kennicutt, and S. A. Macko (1995), Dependance of phytoplankton carbon isotopic composition on growth rate and [CO_2 (aq)]: Theoretical considerations and experimental results, *Geochim. Cosmochim. Acta*, *59*, 1131–1138.

Laws, E. A., R. R. Bidigare, and B. N. Popp (1997), Effect of growth rate and CO_2 concentration on carbon isotopic fractionation by the marine diatom *Phaeodactylum tricornutum*, *Limnol. Oceanogr.*, *42*, 1552–1560.

Lynch-Stieglitz, L., et al. (2007), Atlantic meridional overturning circulation during the last glacial maximum, *Science*, *316*, 66–69.

Madec, G., P. Delecluse, M. Imbard, and C. Lévy (1998), OPA8.1 Ocean general circulation model reference manual, *Notes Sci. Pole Model Climate 11*, 91PP., Inst. Pierre-Simon Laplace, Paris.

Marti, O., et al. (2005), The new IPSL climate system model: IPSL-CM4, *Notes Sci. Pole Model Climat*, *26*, Inst. Pierre-Simon Laplace, Gif sur Yvette, France.

McNeil, B. I., R. J. Matear, and B. Tilbrook (2001), Does carbon 13 track anthropogenic CO2 in the Southern Ocean?, *Global Biogeochem. Cycles*, *15*, 597–613.

O'Leary, T., T. W. Trull, F. B. Griffiths, B. Tilbrook, and A. T. Revill (2001), Euphotic zone variations in the bulk and compound specific $\delta^{13}C$ of suspended organic matter in the subantarctic ocean, south of Australia, *Global Biogeochem. Cycles*, *106*, 31,669–31,684.

Popp, B. N., P. Parekh, B. Tilbrook, R. R. Bidigare, and E. A. Laws (1997), Organic carbon $\delta^{13}C$ variations in sedimentary rocks as chemostratigraphic and paleoenvironmental tools, *Paleogeogr. Paleoclimatol. Paleoecol.*, *132*, 119–132.

Popp, B. N., E. A. Laws, R. R. Bidigare, J. E. Dore, K. L. Hanson, and S. G. Wakeham (1998), Effect of phytoplankton cell geometry on carbon isotopic fractionation, *Geochim. Cosmochim. Acta*, *62*, 69–77.

Popp, B. N., et al. (1999), Controls on the carbon isotopic composition of Southern Ocean phytoplankton, *Global Biogeochem. Cycles*, *13*, 827–843.

Quay, P. D., B. Tilbrook, and C. S. Wong (1992), Oceanic uptake of fossil fuel CO_2: Carbon-13 evidence, *Science*, *256*, 74–79.

Quay, P. D., R. E. Sonnerup, T. Westby, J. Stutsman, and A. P. McNichol (2003), Anthropogenic changes in the 13C/12C of dissolved inorganic carbon in the ocean as a tracer of CO2 uptake, *Global Biogeochem. Cycles*, *17*(1), 1004, doi:10.1029/2001GB001817.

Quay, P. D., R. E. Sonnerup, J. Stutsman, J. Maurer, A. Kortzinger, X. A. Padin, and C. Robinson (2007), Anthropogenic CO2 accumulation rates in the North Atlantic Ocean from changes in the 13C/12C of dissolved inorganic carbon, *Global Biogeochem. Cycles*, *21*, GB1009, doi:10.1029/2006GB002716.

Rau, G. H., U. Riebesell, and D. Wolf-Gladrow (1996), A model of photosynthetic ^{13}C fractionation by marine phytoplankton based on diffusive molecular CO_2 uptake, *Mar. Ecol. Prog. Ser.*, *133*, 275–285.

Raven, J. A., and A. M. Johnston (1991), Mechanisms of inorganic carbon acquisition in marine phytoplankton and their implications for the use of other resources, *Limnol. Oceanogr.*, *36*, 1701–1714.

Rodgers, K. B., J. L. Sarmiento, O. Aumont, C. Crevoisier, C. de Boyer Montegut, and N. Metzl (2008), A wintertime uptake window for anthropogenic CO_2 in the North Pacific, *Global Biogeochem. Cycles*, doi:10.1029/2006GB002920, in press.

Sabine, C. L., et al. (2004), The oceanic sink for anthropogenic CO2, *Science*, *305*, 367–371.

Sarmiento, J. L., et al. (2004), Response of ocean ecosystems to climate warming, *Global Biogeochem. Cycles*, *18*, GB3003, doi:10.1029/2003GB002134.

Sonnerup, R. E., P. D. Quay, A. P. McNichol, J. L. Bullister, T. A. Westby, and H. L. Anderson (1999), Reconstructing the ocean ^{13}C Suess effect, *Global Biogeochem. Cycles*, *13*, 857–872.

Sonnerup, R. E., P. D. Quay, and A. P. McNichol (2000), The Indian Ocean 13C Suess effect, *Global Biogeochem. Cycles*, *14*, 857–873.

Tagliabue, A., L. Bopp, and O. Aumont (2008), Ocean biogeochemistry exhibits contrasting responses to a large scale reduction in dust deposition, *Biogeosciences*, *5*, 11–24.

Tans, P. P., J. A. Berry, and R. F. Keeling (1993), Oceanic $^{12}C/^{13}C$ observation: A new window on ocean CO2 uptake, *Global Biogeochem. Cycles*, *7*, 353–368.

Tortell, P. D., C. L. Martin, and M. E. Corkum (2006), Inorganic carbon uptake and intracellular assimilation by subarctic Pacific phytoplankton assemblages, *Limnol. Oceanogr.*, *51*, 2102–2110.

Timmermann, R., H. Goose, G. Madec, T. Fichefet, C. Ethé, and V. Duliére (2003), On the representation of high latitude processes in the ORCALIM global coupled sea ice-ocean model, *Ocean Modell.*, *8*, 175–201.

Toggweiler, J. R. (1999), Variation of atmospheric CO_2 by ventilation of the ocean's deepest water, *Paleoceanography*, *14*, 571–588.

Trull, T. W., and L. Armand (2001), Insights into Southern Ocean carbon export from the $\delta^{13}C$ of particles and dissolved inorganic carbon during the SOIREE iron release experiment, *Deep Sea Res., Part II*, *48*, 2655–2680.

Wanninkhof, R. (1985), Kinetic fractionation of the carbon isotopes ^{13}C and 12C during the transfer of CO_2 from air to seawater, *Tellus*, *37B*, 128–135.

Wanninkhof, R. (1992), Relationship between wind-speed and gas-exchange over the ocean, *J. Geophys. Res.*, *97*, 7373–7382.

Zhang, J., P. D. Quay, and D. O. Wilbur (1995), Carbon isotope fractionation during gas-water exchange and dissolution of CO_2, *Geochim. Cosmochim. Acta*, *59*, 107–114.

L. Bopp and A. Tagliabue, Laboratoire des Sciences du Climat et de l'Environnement, IPSL-CEA-CNRS-UVSQ Orme des Merisiers, Bat 712, CEA/Saclay, 91198 Gif sur Yvette, France. (alessandro.tagliabue@lsce.ipsl.fr)